

GALOT: Generative Active Learning via Optimizable Zero-shot Text-to-image Generation

Hanbin Hong
University of Connecticut
Storrs, CT 06269

Shenao Yan
University of Connecticut
Storrs, CT 06269

Shuya Feng
University of Connecticut
Storrs, CT 06269

Yan Yan
Illinois Institute of Technology
Chicago, IL 60616

Yuan Hong
University of Connecticut
Storrs, CT 06269

Abstract

Active Learning (AL) represents a crucial methodology within machine learning, emphasizing the identification and utilization of the most informative samples for efficient model training. However, a significant challenge of AL is its dependence on the limited labeled data samples and data distribution, resulting in limited performance. To address this limitation, this paper integrates the zero-shot text-to-image (T2I) synthesis and active learning by designing a novel framework that can efficiently train a machine learning (ML) model solely using the text description. Specifically, we leverage the AL criteria to optimize the text inputs for generating more informative and diverse data samples, annotated by the pseudo-label crafted from text, then served as a synthetic dataset for active learning. This approach reduces the cost of data collection and annotation while increasing the efficiency of model training by providing informative training samples, enabling a novel end-to-end ML task from text description to vision models. Through comprehensive evaluations, our framework demonstrates consistent and significant improvements over traditional AL methods. Codes will be released upon acceptance.

1 Introduction

Active learning is a pivotal technique in machine learning that focuses on selecting and using the most informative samples from a large dataset to train models efficiently [39, 53]. This method significantly reduces the need for labeled data, which lowers labeling costs and speeds up training. However, despite its successes, current active learning strategies are often confined to pre-determined, limited data distributions. This confinement limits the exploration of varied and potentially more insightful data points [55, 44, 18].

Zero-shot text-to-image synthesis models like Stable Diffusion, DELL-E-2, and Imagen provide a novel approach to generating out-of-distribution data. By transforming textual descriptions into visual representations, these models can create expansive datasets of unlabeled

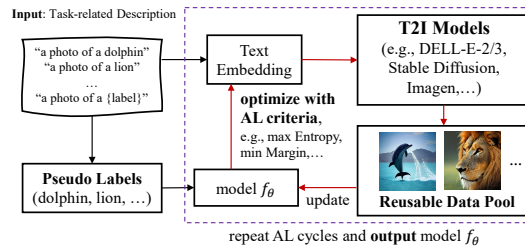


Figure 1: Overview of GALOT. The task-related text is first converted into the text embedding. Then, it iteratively executes 1) optimizing the text embedding according to the AL criteria based on the current model’s output, 2) generating data samples with optimized text embedding, and 3) training the model with generated data and pseudo label. GALOT train the vision model from text inputs.

images [34, 31, 35]. They utilize advanced language models to explore a nearly unlimited embedding space, which is crucial for enhancing Active Learning (AL) strategies [48, 7].

Nevertheless, despite its potential, not all text embeddings yield informative samples, highlighting the need for a selective strategy in choosing and optimizing text inputs. Most of text embeddings might be irrelevant to a specific task, such as utilizing medical images in a cat-dog classification. Moreover, relevant synthetic images may not invariably contribute meaningful information to the learning process [55]. To overcome these challenges, we narrow the scope of text down to task-relevant classes and refine text embedding to produce inherently informative samples (see Figure 1).

The subsequent challenge emerges in the form of annotating the synthetically generated images, a process that traditionally demands substantial manual efforts and resources. Advancements in pre-trained text-to-image models provide a valuable solution. By generating images that accurately reflect their source text, we can assign “pseudo labels” to these images. This approach eliminates the need for manual labeling, thereby reducing labeling costs. Our experiments confirm the high accuracy of these pseudo labels, as detailed in Section 4.4.

Embracing zero-shot text-to-image generation and addressing the identified challenges, our work introduces a novel active learning framework: Generative Active Learning via Optimizable Zero-shot Text-to-image Generation (GALOT). GALOT offers significant advantages over traditional active learning methods:

Data and Annotation Efficiency. By utilizing synthetic data and pseudo-labels, GALOT significantly reduces the need for annotated data. Remarkably, GALOT enables training vision models directly from text inputs, pioneering a *text-to-model* approach (see Figure 1 for illustration). Utilizing accessible online text-to-image models, such as DELL-E-3 [5], lowers barriers for users, allowing them to efficiently train vision models for diverse applications.

Universally-enhanced Learning through Diverse Data Sources. The unlimited variety of text inputs offers a rich source of potentially informative examples. When combined with the active learning strategies, this diversity consistently boosts learning efficiency, as validated in our experiments (Section 4).

Data Reusability and Model Transferability. Despite the initial computational investment, the synthetic dataset can be repurposed across various vision models, often enhancing learning performance without data re-generation (refer to Section 4.3 for experimental insights).

Therefore, in this paper, we made the following primary contributions:

- To our best knowledge, we propose the first paradigm of “*Generative Text-to-Image Active Learning*” that harmonizes active learning with zero-shot text-to-image synthesis. This approach generates informative dataset using textual inputs for training vision models, pioneering a text-to-model approach.
- We propose a novel algorithm that practically refines text inputs and optimizes text embeddings. It leverages the gradients of diffusion models to update the text embedding for generating informative, task-specific data samples.
- We conduct comprehensive experiments on three widely-used datasets under various settings to demonstrate the effectiveness of GALOT. The experimental results, benchmarked with state-of-the-art (SOTA) AL methods, substantiate the efficacy of our proposed generative active learning framework in different aspects.

2 Related Works

Active learning (AL) is a machine learning strategy aimed at improving model accuracy with fewer labeled instances by allowing the model to select the most informative data points for annotation. It is categorized into three types [39]: 1) Pool-based sampling, where the model selects key instances from a large pool of unlabeled data for labeling [39, 12, 38, 50]. 2) Stream-based selective sampling, where instances are evaluated sequentially, and the model determines whether to request labels from an oracle [6, 56, 4]. 3) Membership query synthesis, where the model generates synthetic instances to be labeled by the oracle [2, 55, 44, 25]. Our approach merges membership query synthesis with pool-based sampling, generating data guided by existing instances.

Pseudo-labeling. Pseudo-labeling uses model predictions to label unlabeled data, enhancing training efficiency. However, predictions can be inaccurate, especially in undertrained models, potentially introducing errors into the training set [45, 10]. Our approach differs by utilizing off-the-shelf text-to-image (T2I) models to generate accurate pseudo-labels directly from text inputs.

Data Augmentation and Generative Active Learning. Data augmentation involves creating variations of labeled samples, such as rotations and flips, to improve model generalization and performance [23]. Techniques also include integrating adversarial examples into the training set, enlarging it without additional labeling costs [10]. However, these augmented data instances may not necessarily be informative. Generative Active Learning (GAL) enhances traditional active learning by using generative models like GANs to create synthetic queries for annotation. GAAL [55] pioneered this by using GANs to synthesize samples for active learning queries. BGADL [44] trains a GAN on selected labeled data, then integrates these generated samples into the active learning process without additional annotation costs. In contrast, ASAL [25] uses GANs to generate informative, though not necessarily realistic, samples and then matches them with similar instances from an unlabeled pool. Despite these innovations, studies show that GAL does not consistently match the effectiveness of traditional active learning methods [55, 25] and is often limited to specific machine learning models like Bayesian neural networks [44] or Support Vector Machines [55]. A fundamental issue is that GANs, trained on the distribution of the unlabeled pool, often produce lower-quality data that does not introduce novel, information-rich instances.

Text-to-image Generation. T2I synthesis translates textual descriptions into visual representations, with Reed et al. [33] marking a significant initial advancement by integrating textual semantics into the visual generative process. Subsequent improvements, such as stacked [54], attentional [47], and controllable GANs [22], enhanced image resolution and quality, though challenges like mode collapse persist [14]. Alternative approaches using autoregressive models like DELL-E, Cogview, and Nvwa [32, 9, 46] also demonstrate effective image synthesis.

A major breakthrough in T2I has been achieved with diffusion models, which convert noise into detailed images through a denoising process [15, 42]. Models like Stable Diffusion, DALL-E-2/3, and Imagen [34, 31, 5, 35] excel in generating high-definition, realistic images and show robust zero-shot capabilities, enabling the creation of accurate images from new textual prompts. Despite their high computational demands, these models have revolutionized data synthesis and augmentation [49, 43], providing a foundation for generating diverse image datasets from text.

3 Generative AL via Conditional Diffusion Models

3.1 Active Learning with Data Synthesis

Consider a machine learning model, $f_\theta : \mathbb{R}^d \rightarrow \mathcal{Y}$, where θ denotes the model parameters. Given a loss function \mathcal{L} , the model can be trained using samples $x \in \mathbb{R}^d$ drawn from a data distribution conditioned on s , i.e., $p(x|s)$. The condition s and generated sample x can be in any format, e.g., text, audio, and image, which corresponds to different types of off-the-shelf guided diffusion models [26, 29, 28], which enable the zero-shot generative active learning in different domains. In this paper, we take the text-to-image generation as an example to pursue generative active learning in the image domain. The goal of active learning is to train the model f_θ from scratch using as few labeled data points as possible. Different from traditional active learning [45, 39, 4], our model is trained on the data samples drawn from the data distribution $p(x|s)$.

The optimization problem for vision model training can be formulated as:

$$\theta = \arg \min_{\theta} \mathbb{E}_{x \sim p(x|s)} \mathcal{L}(f_\theta(x), y) \quad (1)$$

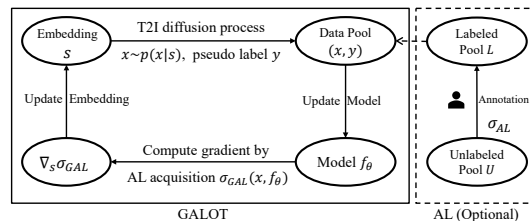


Figure 2: GALOT Workflow for Each Active Learning Cycle. In each active learning cycle, the data sample is generated using pre-trained T2I models with the embedding s and pseudo label. Optionally combined with the traditional AL with real datasets as a complement, the generated data can be used to train a model. The embedding is then optimized according to the updated model via the gradients of the AL acquisition.

where $y \in \mathcal{Y}$ denotes the ground-truth label of the sample x . The goal of the training process is to minimize the loss over the generated sample-label pairs.

3.2 Optimizable Text-to-image Synthesis

Due to the uncertainty when sampling the random data sample from the data distribution and the infinity possibility of the condition s , the unlabeled data pool $\mathcal{U}_{x \sim p(x|s)}$ constructed by the data samples can be considered as an infinite set if the computational resource for sampling data can be infinite. However, not any conditions can generate informative samples that are beneficial for the training, e.g., an image generated from “flower” cannot help distinguish the “dog” and “cat”. Therefore, the condition should be limited to the same domain as the vision task. Also, due to the high computational demand of data synthesis, we aim to generate as few samples as possible by increasing the information in the data samples, which is similar to the goal of active learning.

Traditional active learning methods [39] utilize an acquisition function, $\sigma(\cdot)$, such as the Shannon Entropy [40], to prioritize the selection of informative training samples. Inspired by this idea, we propose to leverage the acquisition function to optimize the text condition to ensure the generated samples are informative. Specifically, we optimize the text embedding to maximize the acquisition function while constraining the text embedding related to the vision task. The text optimization problem can be formally written as:

$$s = \arg \max_s \mathbb{E}_{x \sim p(x|s)} \sigma(x, f_\theta) \quad \text{s.t.} \quad \|s - s^*\|_2 < \epsilon \quad (2)$$

where s^* is a predefined condition related to the specific vision task at hand, and ϵ serves as a regularization term to ensure that the optimized condition does not deviate significantly from the task-related condition.

Predefine Condition. The construction of the predefined text condition s^* is intuitive. Since we are doing the text-to-image data synthesis, we can simply take the label name as the text to compute the text embedding as the predefined text condition. For example, when training a model to classify the CIFAR10 [19], we transform the label names “airplane”, “automobile”, “ship”, etc., to the text embedding for generating corresponding images in these classes. However, in practice, to generate high-quality images using the off-the-shelf T2I models, the text input is supposed to be as detailed as possible. Therefore, we can design some templates for different vision tasks to generate high-quality images, e.g., in our experiments, “a realistic photo of a ship” performs better than simply “ship” (see Section 4.5). Given the template τ , the text condition s_i^* for class i can be computed by a transformation $s_i^* = h_\tau(y_i)$, where y_i is the label of class i . For example, given the template “a photo of a {label}” and the label name “dog”, we simply replace the “{label}” with “dog”, and then using CLIP [30] to encode the text input as text embedding.

Pseudo Label. One of the challenges in generative active learning is the annotation of the generated data. We show that using the text-to-image model for the data synthesis can address this challenge, resulting in annotation-free active learning. Thanks to the advanced zero-shot capability of existing off-the-shelf T2I models [31, 5], the generated image can accurately represent the text input. Therefore, we use the label y_i as the pseudo label for the images generated by s . In the experiments, we show that the accuracy of the pseudo label can be as high as 100% under appropriate templates and embedding distortion (see Section 4.4 for the experimental results).

3.3 Text Optimization on Diffusion Models

Diffusion models [15, 42] typically include two processes for training and generating images, i.e., the forward diffusion process and the reverse diffusion process with each containing multiple steps. The forward diffusion process is used to prepare the target for training the diffusion model. With the reparameterization trick in [15], the variable at the time step x_t can be expressed as:

$$x_t = \sqrt{\bar{\alpha}_t} x_0 + \sqrt{1 - \bar{\alpha}_t} \epsilon \quad (3)$$

where $\bar{\alpha}_t$ is the schedule parameter at t , and $\epsilon \sim \mathcal{N}(0, I)$.

The reverse diffusion process is adopted in the inference stage for generating images, where the variable at time step $t - 1$ is computed from the variable at time step t by denoising. Under the condition s , the reverse diffusion process at each time step t can be defined as $x_{t-1} \sim p(x_{t-1}|x_t, s)$, and the final reversed variable (generated image) x_0 can be expressed as:

Algorithm 1 GALOT Training

1: **Input:** cycle number N , sample number per cycle B_{AL} for AL, sample number per cycle B_{GAL} for GAL, labels y , text perturbation size ϵ , GAL acquisition function σ_{GAL} , AL acquisition function σ_{AL} , text template τ , label-to-text transformation h , classifier f_θ , unlabeled training dataset U , T2I model $M(\cdot)$, text update steps n , and text update stepsize α .
 2: **Output:** model f_θ
 3: **for** cycle = 1 **to** N **do**
 4: Initialize the labeled pool as $L = \emptyset$
 5: Select top B_{AL} samples from U ranked by σ_{AL} as the batch V and add to the labeled pool $L = L \cup V$
 6: Compute the predefined text embedding: $s^* = h_\tau(y)$
 7: Initialize text embedding $s = s^*$
 8: Optimize text embedding: $s' = \text{TextOpt}(s, s^*, \epsilon, \alpha, n, \sigma_{GAL}, f_\theta)$
 9: Generate B_{GAL} input pairs $G = \{x, \hat{y}\}$ with $x = M(s')$ and pseudo label $\hat{y} = y$.
 10: Train the model f_θ with $L \cup G$
 11: **end for**

$$x_0 \sim p(x_{0:T-1}|x_T, s) = \prod_{t=T}^1 p(x_{t-1}|x_t, s) \quad (4)$$

where T denotes the total time step.

Suppose we have white-box access to the pre-trained T2I diffusion models, to optimize the text embedding, one promising solution is to use the gradient descent, e.g., Projected Gradient Descent (PGD) [24]. In this way, we update the text embedding s according to the gradients:

$$s_i = s_{i-1} + \alpha \text{sgn}[\mathbb{E}_{x_0 \sim p(x_{0:T-1}|x_T, s)} \nabla_s \sigma(x_0, f_\theta)] \quad (5)$$

$$s.t. \quad \|s_i - s^*\|_2 \leq \epsilon \quad (6)$$

where $i = 1, 2, \dots, k$ denotes the updating step, α denotes the step size, $\text{sgn}[\cdot]$ denotes the sign function. However, computing the gradient $\nabla_s \sigma(x_0, f_\theta)$ is extremely challenging even with the auto-gradient techniques in ML libraries, e.g., Pytorch [27] or TensorFlow [1], due to the recurrent denoising steps. By Proposition 1, we make it feasible to estimate the gradients using the auto-gradient.

Proposition 1. Assume Eq. (3) holds in the reverse diffusion process, then the gradient can be written as:

$$\nabla_s \sigma(x_0, f_\theta) = T \nabla_{x_0} \sigma \cdot J_{x_0, s} \quad (7)$$

where $J_{x_0, s}$ denotes the Jacobian of x_0 w.r.t. s .

Proof. Note that each reverse diffusion step is conditioned on the text condition s , so the gradient should be computed as the summation:

$$\nabla_s \sigma(x_0, f_\theta) = \sum_{t=0}^T \nabla_{x_t} \sigma \cdot J_{x_t, s} \quad (8)$$

$$= \sum_{t=0}^T \nabla_{x_0} \sigma \cdot J_{x_0, x_t} \cdot J_{x_t, x_0} \cdot J_{x_0, s} \quad (9)$$

$$\text{(by Eq. (3))} = T \nabla_{x_0} \sigma \cdot J_{x_0, s} \quad (10)$$

Thus, this completes the proof. \square

The gradients $\nabla_{x_0} \sigma \cdot J_{x_0, s}$ can be efficiently computed by the auto-gradient through the graph of *the last reverse diffusion step*. The assumption that Eq. (3) holds is based on the empirical observation that off-the-shelf T2I models are trained to approximate this equality in the reverse process.

3.4 GAL-AL Joint Sampling

Without consuming any annotation budget, our method can achieve moderate performance on zero-shot classification (see Section 4.2 for the experimental results), however, to train a model targeting the high performance on a test set in a specific task, the real training data can be helpful. Therefore, we combine the generated samples (without annotation) and the real samples (with annotation) to train the model, leading to significantly boosted performance on the test set compared with the model solely trained on the training set.

The algorithms for generative active learning are presented in Algorithm 1 (also see Figure 2 for the summarized workflow). *TextOpt* function follows Eq. (5) to optimize the text embedding. We estimate the expectation of the gradients using the average gradients over k generated samples.

4 Experimental Results

In this section, we comprehensively evaluate the proposed generative active learning framework. First, we benchmark GALOT with the SOTA AL baselines. Second, we evaluate the performance of GALOT when the model is trained solely on the generated data without real data. Third, we evaluate the reusability and the transferability of the generated data. Fourth, we evaluate the performance of the pseudo-labeling by human annotation. Finally, we conduct 7 various ablation studies to evaluate the effectiveness of each component of GALOT. Visualized examples can be found in Appendix B.

Datasets. We evaluate our model using three established image datasets of varying scales: CIFAR10/100 [19], and TinyImageNet [20]. CIFAR10 includes 60,000 32x32 color images across 10 classes, suitable for basic image recognition tasks. CIFAR100 expands this to 100 classes with the same image count, offering a more complex classification challenge. TinyImageNet, a condensed version of the larger ImageNet dataset [8], comprises 100,000 training, 10,000 validation, and 10,000 testing images in 64x64 resolution across 200 classes, providing a diverse and challenging environment for testing.

Experimental Setting. GALOT is based on the off-the-shelf Text-to-Image models for generating data points. Specifically, we use Stable Diffusion [34] pre-trained model (version 2.1 base ¹) in all the experiments. Other pre-trained models like Imagen [35], or other online platforms like DELL-E-3 ² can also be used for zero-shot GAL w/wo the text optimization. In all the experiments, we set the diffusion step T as 50, and the sampling number for gradient estimation k as 6. The resolution of the generated images is 512×512 by default and further resized to match different datasets. In all the experiments, unless otherwise stated, we use GAL-AL joint sampling, set ResNet18 as the classifier architecture, and set ϵ to linearly grow from 0 to 0.5. The detailed parameter setting for each section is summarized in Appendix A for thorough reference and clarity.

Experimental Environment. We implement GALOT in PyTorch [27] based on open-source libraries Diffusers ³ and DeepALPlus ⁴ [53]. The experiments were running on a server with AMD EPYC Genoa 9354 CPUs (32 Core, 3.3GHz), and NVIDIA H100 Hopper GPUs (80GB each).

4.1 GALOT vs. SOTA Active Learning Methods

We first present a comprehensive comparison of model performance between GALOT and state-of-the-art (SOTA) AL approaches (12 methods). To evaluate the efficiency of the text embedding refinement, we also evaluate a basic version of GALOT, denoted as “GALOT (basic)”, where it only considers the basic text template without text optimization. For all three datasets, we perform $N = 10$ cycle of active learning with a ResNet18 classifier (except for the GAAL [55] which only support SVM). The sampling number per cycle for the SOTA active learning methods is set to $B_{AL} = 1,000$, resulting in a 10,000 total annotation number. For GALOT and its basic version, we additionally generate $B_{GAL} = |L|$ number of samples for each cycle without consuming the annotation budget. We measure the prediction accuracy on the test set of each dataset.

As is shown in Table 1, none of the SOTA methods shows dominant performance over other methods. However, our GALOT and its basic version consistently outperforms SOTA methods in all the settings. This is a significant achievement, indicating the robustness and efficiency of GALOT. The superior performance of GALOT is due to the additional informative data generated by T2I models with pseudo-labels, leading to a minimum improvement of 0.72% and a maximum improvement of 8.78% over SOTA methods. The average improvement on CIFAR10, CIFAR100, and TinyImageNet are 3.84%, 7.71%, and 3.29%, respectively. This indicates our GALOT can serve as an orthogonal method to boost the performance of active learning methods universally. It is worth noting that the GALOT outperforms GALOT (basic) by as much as 5.86% on CIFAR10, indicating the superiority of the text refinement. On TinyImageNet, GALOT and GALOT (basic) give similar accuracies due to the high complexity of text embedding space (TinyImageNet has 200 classes) but still demonstrate significant improvement over AL baselines.

¹<https://huggingface.co/stabilityai/stable-diffusion-2-1-base>

²<https://openai.com/dall-e-3>

³<https://github.com/huggingface/diffusers>

⁴<https://github.com/SineZHAN/deepALplus>

Table 1: Comparison with SOTA AL. We present the accuracy on the test set vs. different annotation budget $|L|$. The first column presents the dataset and the fully-supervised accuracy. The last column presents the average accuracy over all settings.

Dataset	Method	1000	2000	3000	4000	5000	6000	7000	8000	9000	10000	Average
CIFAR-10 (0.9536)	GAAL [55]	0.2811	0.2132	0.2086	0.2140	0.2086	0.1991	0.2005	0.2012	0.1981	0.2011	0.2126
	RandomSampling	0.5498	0.6631	0.7347	0.7912	0.8195	0.8369	0.8513	0.8645	0.8789	0.8841	0.7874
	EntropySampling [39]	0.5466	0.6718	0.7797	0.8109	0.8460	0.8580	0.8876	0.8901	0.9013	0.9063	0.8098
	MarginSampling [37]	0.5506	0.6800	0.8127	0.8127	0.8400	0.8546	0.8830	0.8927	0.9058	0.9049	0.8137
	LeastConfidence [21]	0.5591	0.6790	0.7661	0.8111	0.8481	0.8640	0.8790	0.8932	0.9035	0.9145	0.8118
	BALD [13]	0.5589	0.6591	0.7612	0.8184	0.8481	0.8654	0.8788	0.8897	0.9019	0.9077	0.8089
	BADGE [3]	0.5592	0.6882	0.7698	0.8160	0.8458	0.8582	0.8774	0.8877	0.9006	0.9049	0.8108
	MeanSTD [17]	0.5350	0.7046	0.7393	0.8116	0.8398	0.8679	0.8828	0.8909	0.8971	0.9093	0.8078
	VarRatio [11]	0.5534	0.6616	0.7733	0.8045	0.8413	0.8682	0.8813	0.8995	0.8994	0.9079	0.8090
	KMeans	0.5594	0.6646	0.7381	0.7807	0.8078	0.8347	0.8516	0.8623	0.8743	0.8800	0.7854
	CoreSet [38]	0.5529	0.6748	0.7477	0.8056	0.8361	0.8534	0.8739	0.8866	0.8951	0.9024	0.8029
	LossPrediction [51]	0.5291	0.6319	0.7205	0.7366	0.7688	0.8252	0.8523	0.7977	0.8786	0.8829	0.7624
	GALOT (basic)	0.5874	0.7162	0.7966	0.8288	0.8631	0.8790	0.8937	0.9012	0.9133	0.9179	0.8297
	GALOT	0.6460	0.7551	0.8245	0.8594	0.8763	0.8958	0.9073	0.9130	0.9188	0.9246	0.8521
Improvement	+0.0878	+0.0505	+0.0118	+0.0410	+0.0282	+0.0276	+0.0197	+0.0135	+0.0130	+0.0101	+0.0384	
CIFAR-100 (0.7668)	RandomSampling	0.1408	0.2080	0.2656	0.3086	0.3635	0.3995	0.4418	0.4703	0.4973	0.5250	0.3620
	EntropySampling [39]	0.1442	0.1938	0.2474	0.2957	0.3517	0.3851	0.4161	0.4441	0.4839	0.5379	0.3500
	MarginSampling [37]	0.1482	0.1985	0.2528	0.3155	0.3788	0.4056	0.4476	0.4951	0.5237	0.5343	0.3700
	LeastConfidence [21]	0.1448	0.1938	0.2521	0.3087	0.3553	0.3830	0.4216	0.4545	0.4981	0.5415	0.3553
	BALD [13]	0.1450	0.2012	0.2644	0.3099	0.3553	0.3960	0.4245	0.4634	0.4880	0.5274	0.3575
	BADGE [3]	0.1441	0.2066	0.2644	0.3137	0.3857	0.4164	0.4462	0.4810	0.5094	0.5507	0.3718
	MeanSTD [17]	0.1434	0.2016	0.2673	0.3221	0.3560	0.3877	0.4298	0.4573	0.4837	0.5270	0.3576
	VarRatio [11]	0.1447	0.1954	0.2463	0.3026	0.3480	0.3807	0.4316	0.4725	0.4829	0.5415	0.3546
	KMeans	0.1462	0.2137	0.2707	0.3261	0.3631	0.3863	0.4165	0.4521	0.4833	0.5052	0.3563
	CoreSet [38]	0.1424	0.2059	0.2560	0.3169	0.3646	0.3988	0.4413	0.4972	0.5164	0.5483	0.3688
	LossPrediction [51]	0.1322	0.1780	0.2387	0.2988	0.3275	0.3507	0.4143	0.4126	0.4444	0.4566	0.3254
	GALOT (basic)	0.1669	0.2713	0.3310	0.3885	0.4474	0.4777	0.5105	0.5411	0.5629	0.5943	0.4292
	GALOT	0.1892	0.2893	0.3585	0.4170	0.4683	0.4921	0.5346	0.5619	0.5807	0.5974	0.4489
	Improvement	+0.0410	+0.0756	+0.0878	+0.0909	+0.0826	+0.0757	+0.0870	+0.0647	+0.0570	+0.0467	+0.0771
TinyImageNet (0.5054)	RandomSampling	0.1279	0.1944	0.2327	0.2617	0.2574	0.3064	0.3348	0.3477	0.3604	0.3613	0.2785
	EntropySampling [39]	0.1256	0.1809	0.2152	0.2399	0.2222	0.2817	0.3159	0.3149	0.3378	0.3313	0.2565
	MarginSampling [37]	0.1274	0.1764	0.2290	0.2496	0.2350	0.3029	0.3137	0.3355	0.3517	0.3472	0.2668
	LeastConfidence [21]	0.1269	0.1799	0.2187	0.2427	0.2223	0.2909	0.3031	0.3152	0.3351	0.3291	0.2564
	BALD [13]	0.1282	0.1877	0.2230	0.251	0.2466	0.2942	0.3142	0.3263	0.3364	0.3387	0.2646
	BADGE [3]	0.1278	0.1858	0.2350	0.2651	0.2467	0.3073	0.3190	0.3410	0.3562	0.3518	0.2736
	MeanSTD [17]	0.1253	0.1815	0.2250	0.2447	0.2422	0.2920	0.3123	0.3279	0.3320	0.3351	0.2618
	VarRatio [11]	0.1288	0.1736	0.2025	0.2429	0.2222	0.2915	0.2997	0.3061	0.3280	0.3279	0.2523
	KMeans	0.1259	0.1965	0.2329	0.2704	0.2546	0.3153	0.3329	0.3510	0.3633	0.3552	0.2798
	CoreSet [38]	0.1274	0.1793	0.2114	0.2441	0.2258	0.2944	0.3092	0.3209	0.3358	0.3348	0.2583
	LossPrediction [51]	0.0424	0.0599	0.0778	0.1113	0.1136	0.1427	0.1500	0.1654	0.1800	0.1775	0.1221
	GALOT (basic)	0.1660	0.2332	0.2805	0.3087	0.3134	0.3540	0.3566	0.3683	0.3730	0.3790	0.3133
	GALOT	0.1681	0.2316	0.2812	0.3109	0.3158	0.3481	0.3562	0.3665	0.3705	0.3783	0.3127
	Improvement	+0.0393	+0.0367	+0.0462	+0.0405	+0.0584	+0.0387	+0.0218	+0.0173	+0.0097	+0.0177	+0.0335

4.2 GAL-AL Joint Sampling

In this section, we benchmark our GAL-AL joint sampling (“AL+GAL”) with 1) Baseline AL: the traditional pool-based AL baseline, which solely relies on labeled samples for training; 2) Baseline GAL: the GAL baseline that solely relies on the generated samples for training; 3) Baseline Fully-supervised: the fully-supervised baseline that trains the model with full training dataset. Detailed settings on experimental parameters can be found in Appendix A.

As is shown in Figure 3, we surprisingly observe that Baseline GAL achieves an accuracy as high as 58.63% on CIFAR10. It is worth noting that the training does not require any real training data, but only relies on the knowledge about the vision task (text inputs). It provides a potential solution to train a model from scratch without any data and labeling. This kind of text-to-model capability stems from the zero-shot representation of large language models and the high-fidelity generation of diffusion models, addressing the high cost of labeling, and data collection. Combining the synthesized samples with the labeled samples, GALOT significantly improves the performance of SOTA active learning for free (without additional annotation). On CIFAR10, GAL-AL can achieve 92.46% accuracy (2.9% gap to the fully-supervised learning) with only 10,000 labels.

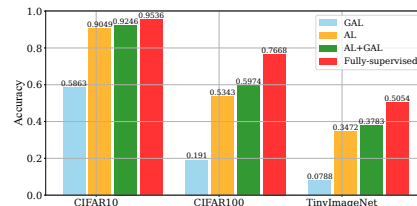


Figure 3: Comparison of Different Baselines.

4.3 Dataset Reuse and Transferability

In this experiment, we train different models on the generated dataset in Section 4.1 to illustrate the data transferability over different models. We focus on four distinct models, which vary in size and architecture: VGG16 [41], DenseNet121 [16], MobileNetV2 [36] and DLA [52]. Table 2 presents

Table 2: Data Reuse for Different Networks on CIFAR10.

Model	1000	2000	3000	4000	5000	6000	7000	8000	9000	10000	Average
MarginSampling	0.5506	0.6800	0.8127	0.8127	0.8400	0.8546	0.8830	0.8927	0.9058	0.9049	0.8137
LeastConfidence	0.5591	0.6790	0.7661	0.8111	0.8481	0.8640	0.8790	0.8932	0.9035	0.9145	0.8118
Baseline (Resnet 18)	0.6460	0.7551	0.8245	0.8594	0.8763	0.8958	0.9073	0.9130	0.9188	0.9246	0.8521
VGG16	0.6597	0.7687	0.8069	0.8362	0.8587	0.8746	0.8834	0.8903	0.8915	0.9029	0.8373
DenseNet121	0.6571	0.7832	0.8434	0.8569	0.8872	0.8969	0.9143	0.9199	0.9276	0.9359	0.8622
MobileNetv2	0.6551	0.7689	0.8137	0.8491	0.8729	0.8881	0.8996	0.9093	0.9196	0.9214	0.8498
DLA	0.6634	0.7747	0.8161	0.8546	0.8731	0.8873	0.8986	0.9080	0.9184	0.9252	0.8519

the transferability results, showcasing various models’ performance when trained on the generated dataset. The first two rows present the traditional AL results, and the third row is the results of GALOT as the same in Table 1. The following rows show the performance of different models when trained on the data generated for ResNet18.

The data presented in the table reveals that all four models trained on the reused dataset surpass the two baseline AL methods in terms of average model accuracy. Notably, with the exception of VGG16, all other models even exceed the baseline active learning methods in model accuracy after each training cycle. This indicates that the dataset generated by GALOT demonstrates significant reusability and transferability. Compared to Baseline (Resnet 18), models like DenseNet121, MobileNetV2, and DLA not only demonstrate superior average accuracy but also higher accuracy after each training round. This improved performance is likely due to the inherent advantages of their architectural designs. In conclusion, Table 2 demonstrates that the GALOT can generate informative data that is not specific to a model but general for a task (or multiple tasks).

4.4 Performance of Pseudo-labeling via Human Annotation

To evaluate the efficacy of pseudo-labels generated by our model, we compute the accuracy of the pseudo-label through human annotation. Specifically, for each template, we randomly optimize the text embedding under the constraint of various ϵ . The generated image is marked as correct when it accurately represents the pseudo-label. We evaluate the accuracy for 100 images on each setting. In Figure 4, we observe that descriptive templates like “a photo of a {label}” demonstrated higher robustness, maintaining high accuracy even at higher distortion levels. In contrast, simpler templates, particularly “label”, were more susceptible to distortion, showing a marked decrease in accuracy. These results underscore the significance of prompt complexity in maintaining the fidelity of generative models under varying conditions, highlighting the need for well-structured prompts in enhancing model robustness.

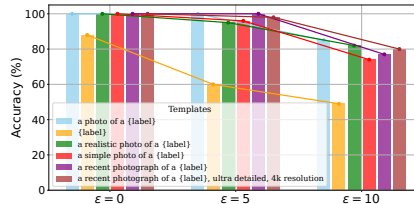


Figure 4: Text-to-image Generation Accuracy (Human Evaluated) vs. ϵ with Different Templates.

4.5 Ablation Study

Table 3: Comparison of Different Text Templates on CIFAR10.

Text Template	1000	2000	3000	4000	5000	Average
"a photo of a {label}"	0.6091 ± 0.0032	0.7388 ± 0.0051	0.8103 ± 0.0030	0.8403 ± 0.0031	0.8638 ± 0.0036	0.7642 ± 0.0085
"{label}"	0.5566 ± 0.0072	0.6969 ± 0.001	0.7921 ± 0.0015	0.8312 ± 0.0001	0.8525 ± 0.0005	0.7521 ± 0.0077
"a realistic photo of a {label}"	0.6074 ± 0.0049	0.7279 ± 0.0015	0.8049 ± 0.0054	0.8489 ± 0.0015	0.8644 ± 0.0026	0.7642 ± 0.0039
"a simple photo of a {label}"	0.6043 ± 0.0025	0.7466 ± 0.0067	0.8063 ± 0.0036	0.8367 ± 0.0033	0.8607 ± 0.0027	0.7718 ± 0.0005
"a recent color photograph of a {label}"	0.5998 ± 0.0032	0.7475 ± 0.0061	0.8051 ± 0.0030	0.8459 ± 0.0011	0.8682 ± 0.0020	0.7721 ± 0.0002
"a recent color photograph of a {label}, ultra detailed, ..."	0.5842 ± 0.0062	0.7361 ± 0.0009	0.7986 ± 0.0057	0.8328 ± 0.0032	0.8667 ± 0.0035	0.7672 ± 0.0000

Text Template Comparisons for CIFAR10. In this section, we evaluate the performance of GALOT versus various different text templates. The text input is constructed using different text templates in Table 3 by replacing “{label}” with the label name of each class. In Table 3, it is observed that none of the templates dominate over all annotation budgets. However, the templates "a realistic photo of a {label}" and "a simple photo of a {label}" generally perform better than other templates, while simply using "{label}" as the template results in the worse performance on average. This indicates that using appropriate text templates to generate the image can improve the image generation quality (see Section 4.4 for more results) and further improve the learning.

ϵ in Text Embedding Optimization. The impact of varying values of ϵ on text embedding optimization is illustrated in Table 4. The results show that using $\epsilon > 0$ can achieve better performance than setting $\epsilon = 0$, except for the $|L| = 1,000$ setting. This indicates that the text embedding optimization is effective.

Table 4: Ablation study of ϵ .

Method	ϵ	1000	2000	3000	4000	5000
GALOT w/o Opt	0	0.6547	0.7700	0.8228	0.8497	0.8733
GALOT w/ Opt	0.25	0.6396	0.7675	0.8275	0.8576	0.8739
GALOT w/ Opt	0.50	0.6440	0.7676	0.8278	0.8627	0.8795
GALOT w/ Opt	1.00	0.6407	0.7549	0.8213	0.8608	0.8764
GALOT w/ Opt	10.00	0.6224	0.7702	0.8111	0.8471	0.8655

Acquisition Function σ_{GAL} . In this study, we assessed the effectiveness of four acquisition functions for GAL in GALOT: random sampling, entropy sampling, margin sampling, and least confidence. According to the results presented in Figure 5, random sampling demonstrates superior performance, particularly in the last three cycles. While this might seem unconventional, a similar trend has been observed on TinyImageNet in Table 1. It is probably when the model is not well-trained, that the guidance of the AL acquisition function is meaningless, since when the model predicts more accurately (see CIFAR10 and CIFAR100 in Table 1), other acquisition function gradually outperforms the random sampling.

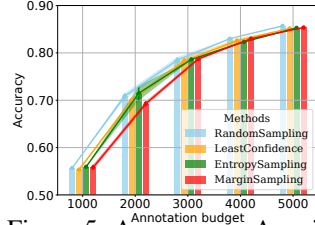


Figure 5: Accuracy vs Acquisition Methods σ_{GAL} .

Sampling Number B_{GAL} vs. Annotation Budgets. In this experiment, we examine the effects of the number of generated samples on the performance of GALOT. We generate $0.5|L|$, $|L|$, and $1.5|L|$ data samples for GALOT. The results are presented in Figure 6. The performance with different B_{GAL} does not vary a lot because, in the same cycle, all the B_{GAL} samples are generated with the same text embedding, thus cannot provide new data distribution, resulting in a similar performance.

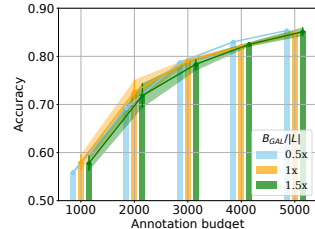


Figure 6: Accuracy vs B_{GAL} .

Table 5: Training Scale Comparison

Methods	1000	2000	3000	4000	5000
MarginSampling (300 epochs)	0.5578	0.6686	0.7369	0.8001	0.8383
MarginSampling (600 epochs)	0.5730	0.6810	0.7793	0.8356	0.8529
GALOT (300 epochs)	0.6460	0.7551	0.8245	0.8594	0.8763

Table 6: Extra Generation

Method	1000	2000	3000	4000	5000
Gen 1L/ Sample 1L	0.6460	0.7551	0.8245	0.8594	0.8763
Gen 21L/ Sample 1L	0.6504	0.7563	0.8279	0.8517	0.8764

Training Scale Comparison. Since GALOT uses additional synthesized datasets during the training, compared to the standard training, GALOT may introduce more training iterations, although the annotation budget is the same. This brings potential uncertainty to the validation of the improvement. Therefore, to explicitly quantify the improvement caused by the better data distribution, we train the AL baseline with the same iteration as ours. Table 5 shows that increasing the training iteration of AL baselines improves the performance slightly, but GALOT still drastically outperforms the AL baseline.

Extra Generation. GALOT can generate as many as possible samples if the computational resource allows, therefore, we also evaluate the performance when generating $2|L|$ samples while randomly selecting $|L|$ samples. Table 6 shows that generating more samples and randomly selecting half of them can lead to slightly performance improvement.

Different σ_{AL} and σ_{GAL} . We also test various σ_{AL} and σ_{GAL} on GALOT. This is different from the ablation study of varying σ_{GAL} , where the acquisition function for the AL baseline is fixed on margin sampling. From Table 7, it is observed that when using margin sampling for both the σ_{AL} and σ_{GAL} , the performance is better.

Table 7: Different σ_{AL} and σ_{GAL} .

Strategy	1000	2000	3000	4000	5000
MarginSampling	0.6460	0.7551	0.8245	0.8594	0.8763
RandomSampling	0.6297	0.7615	0.8071	0.8382	0.8580
EntropySampling	0.6358	0.7490	0.8212	0.8581	0.8811

5 Conclusion

Our innovative framework GALOT successfully merges AL with T2I synthesis, overcoming traditional AL’s data limitations. By optimizing text embeddings to generate informative samples, GALOT broadens data diversity and training efficiency, pioneering the text-to-model approaches. Our evaluations demonstrate its superiority over existing AL methods, marking a significant step forward in developing generative active learning with zero-shot T2I generation.

References

- [1] Abadi, M., Agarwal, A., Barham, P., Brevdo, E., Chen, Z., Citro, C., Corrado, G.S., Davis, A., Dean, J., Devin, M., et al.: Tensorflow: Large-scale machine learning on heterogeneous distributed systems. arXiv preprint arXiv:1603.04467 (2016)
- [2] Angluin, D.: Queries and concept learning. *Mach. Learn.* **2**(4), 319–342 (1987). <https://doi.org/10.1007/BF00116828>, <https://doi.org/10.1007/BF00116828>
- [3] Ash, J.T., Zhang, C., Krishnamurthy, A., Langford, J., Agarwal, A.: Deep batch active learning by diverse, uncertain gradient lower bounds. arXiv preprint arXiv:1906.03671 (2019)
- [4] Bachman, P., Sordoni, A., Trischler, A.: Learning algorithms for active learning. In: 5th International Conference on Learning Representations, ICLR 2017, Toulon, France, April 24-26, 2017, Workshop Track Proceedings. OpenReview.net (2017), <https://openreview.net/forum?id=rJj2ZxHt1>
- [5] Betker, J., Goh, G., Jing, L., Brook, T., Wang, J., Li, L., Ouyang, L., Zhuang, J., Lee, J., Guo, Y., Manassra, W., Dhariwal, P., Chu, C., Jiao, Y., Ramesh, A.: Improving image generation with better captions. <https://cdn.openai.com/papers/dall-e-3.pdf> (2023)
- [6] Cohn, D.A., Atlas, L.E., Ladner, R.E.: Improving generalization with active learning. *Mach. Learn.* **15**(2), 201–221 (1994). <https://doi.org/10.1007/BF00993277>, <https://doi.org/10.1007/BF00993277>
- [7] Croitoru, F.A., Hondru, V., Ionescu, R.T., Shah, M.: Diffusion models in vision: A survey. *IEEE Transactions on Pattern Analysis and Machine Intelligence* (2023)
- [8] Deng, J., Dong, W., Socher, R., Li, L.J., Li, K., Fei-Fei, L.: Imagenet: A large-scale hierarchical image database. In: 2009 IEEE conference on computer vision and pattern recognition. pp. 248–255. Ieee (2009)
- [9] Ding, M., Yang, Z., Hong, W., Zheng, W., Zhou, C., Yin, D., Lin, J., Zou, X., Shao, Z., Yang, H., Tang, J.: Cogview: Mastering text-to-image generation via transformers. In: Ranzato, M., Beygelzimer, A., Dauphin, Y.N., Liang, P., Vaughan, J.W. (eds.) *Advances in Neural Information Processing Systems 34: Annual Conference on Neural Information Processing Systems 2021, NeurIPS 2021, December 6-14, 2021, virtual*. pp. 19822–19835 (2021), <https://proceedings.neurips.cc/paper/2021/hash/a4d92e2cd541fca87e4620aba658316d-Abstract.html>
- [10] Ducoffe, M., Precioso, F.: Adversarial active learning for deep networks: a margin based approach. *CoRR* **abs/1802.09841** (2018), <http://arxiv.org/abs/1802.09841>
- [11] Freeman, L.C.: Elementary applied statistics: for students in behavioral science. (No Title) (1965)
- [12] Gal, Y., Islam, R., Ghahramani, Z.: Deep bayesian active learning with image data. In: Precup, D., Teh, Y.W. (eds.) *Proceedings of the 34th International Conference on Machine Learning, ICML 2017, Sydney, NSW, Australia, 6-11 August 2017. Proceedings of Machine Learning Research*, vol. 70, pp. 1183–1192. PMLR (2017), <http://proceedings.mlr.press/v70/gal17a.html>
- [13] Gal, Y., Islam, R., Ghahramani, Z.: Deep Bayesian active learning with image data. In: *Proceedings of the 34th International Conference on Machine Learning*. PMLR (2017)
- [14] Goodfellow, I.J., Pouget-Abadie, J., Mirza, M., Xu, B., Warde-Farley, D., Ozair, S., Courville, A.C., Bengio, Y.: Generative adversarial nets. In: Ghahramani, Z., Welling, M., Cortes, C., Lawrence, N.D., Weinberger, K.Q. (eds.) *Advances in Neural Information Processing Systems 27: Annual Conference on Neural Information Processing Systems 2014, December 8-13 2014, Montreal, Quebec, Canada*. pp. 2672–2680 (2014), <https://proceedings.neurips.cc/paper/2014/hash/5ca3e9b122f61f8f06494c97b1afccf3-Abstract.html>

- [15] Ho, J., Jain, A., Abbeel, P.: Denoising diffusion probabilistic models. In: Larochelle, H., Ranzato, M., Hadsell, R., Balcan, M., Lin, H. (eds.) *Advances in Neural Information Processing Systems 33: Annual Conference on Neural Information Processing Systems 2020, NeurIPS 2020*, December 6-12, 2020, virtual (2020), <https://proceedings.neurips.cc/paper/2020/hash/4c5bcfec8584af0d967f1ab10179ca4b-Abstract.html>
- [16] Huang, G., Liu, Z., Van Der Maaten, L., Weinberger, K.Q.: Densely connected convolutional networks. In: *Proceedings of the IEEE conference on computer vision and pattern recognition*. pp. 4700–4708 (2017)
- [17] Kampffmeyer, M., Salberg, A.B., Jenssen, R.: Semantic segmentation of small objects and modeling of uncertainty in urban remote sensing images using deep convolutional neural networks. In: *Proceedings of the IEEE conference on computer vision and pattern recognition workshops*. pp. 1–9 (2016)
- [18] Kim, Y.Y., Song, K., Jang, J., Moon, I.C.: Lada: Look-ahead data acquisition via augmentation for deep active learning. *Advances in Neural Information Processing Systems* **34**, 22919–22930 (2021)
- [19] Krizhevsky, A., Hinton, G., et al.: Learning multiple layers of features from tiny images (2009)
- [20] Le, Y., Yang, X.: Tiny imagenet visual recognition challenge. *CS 231N* **7**(7), 3 (2015)
- [21] Lewis, D.D., Gale, W.A.: A sequential algorithm for training text classifiers. In: *Proceedings of the 17th Annual International ACM-SIGIR Conference on Research and Development in Information Retrieval*. ACM/Springer (1994)
- [22] Li, B., Qi, X., Lukasiewicz, T., Torr, P.H.S.: Controllable text-to-image generation. In: Wallach, H.M., Larochelle, H., Beygelzimer, A., d’Alché-Buc, F., Fox, E.B., Garnett, R. (eds.) *Advances in Neural Information Processing Systems 32: Annual Conference on Neural Information Processing Systems 2019, NeurIPS 2019*, December 8-14, 2019, Vancouver, BC, Canada. pp. 2063–2073 (2019), <https://proceedings.neurips.cc/paper/2019/hash/1d72310edc006dadf2190caad5802983-Abstract.html>
- [23] Ma, Y., Lu, S., Xu, E., Yu, T., Zhou, L.: Combining active learning and data augmentation for image classification. In: *ICBDT 2020: 3rd International Conference on Big Data Technologies*, Qingdao, China, September, 2020. pp. 58–62. ACM (2020). <https://doi.org/10.1145/3422713.3422726>, <https://doi.org/10.1145/3422713.3422726>
- [24] Madry, A., Makelov, A., Schmidt, L., Tsipras, D., Vladu, A.: Towards deep learning models resistant to adversarial attacks. In: *International Conference on Learning Representations* (2018)
- [25] Mayer, C., Timofte, R.: Adversarial sampling for active learning. In: *IEEE Winter Conference on Applications of Computer Vision, WACV 2020, Snowmass Village, CO, USA, March 1-5, 2020*. pp. 3060–3068. IEEE (2020). <https://doi.org/10.1109/WACV45572.2020.9093556>, <https://doi.org/10.1109/WACV45572.2020.9093556>
- [26] Nichol, A.Q., Dhariwal, P., Ramesh, A., Shyam, P., Mishkin, P., McGrew, B., Sutskever, I., Chen, M.: GLIDE: towards photorealistic image generation and editing with text-guided diffusion models. In: Chaudhuri, K., Jegelka, S., Song, L., Szepesvári, C., Niu, G., Sabato, S. (eds.) *International Conference on Machine Learning, ICML 2022, 17-23 July 2022, Baltimore, Maryland, USA. Proceedings of Machine Learning Research*, vol. 162, pp. 16784–16804. PMLR (2022), <https://proceedings.mlr.press/v162/nichol22a.html>
- [27] Paszke, A., Gross, S., Massa, F., Lerer, A., Bradbury, J., Chanan, G., Killeen, T., Lin, Z., Gimelshein, N., Antiga, L., et al.: Pytorch: An imperative style, high-performance deep learning library. *Advances in neural information processing systems* **32** (2019)
- [28] Poole, B., Jain, A., Barron, J.T., Mildenhall, B.: Dreamfusion: Text-to-3d using 2d diffusion. In: *The Eleventh International Conference on Learning Representations, ICLR 2023, Kigali, Rwanda, May 1-5, 2023*. OpenReview.net (2023), <https://openreview.net/pdf?id=FjNys5c7VyY>

- [29] Popov, V., Vovk, I., Gogoryan, V., Sadekova, T., Kudinov, M.A.: Grad-tts: A diffusion probabilistic model for text-to-speech. In: Meila, M., Zhang, T. (eds.) Proceedings of the 38th International Conference on Machine Learning, ICML 2021, 18-24 July 2021, Virtual Event. Proceedings of Machine Learning Research, vol. 139, pp. 8599–8608. PMLR (2021), <http://proceedings.mlr.press/v139/popov21a.html>
- [30] Radford, A., Kim, J.W., Hallacy, C., Ramesh, A., Goh, G., Agarwal, S., Sastry, G., Askell, A., Mishkin, P., Clark, J., et al.: Learning transferable visual models from natural language supervision. In: International conference on machine learning. pp. 8748–8763. PMLR (2021)
- [31] Ramesh, A., Dhariwal, P., Nichol, A., Chu, C., Chen, M.: Hierarchical text-conditional image generation with clip latents. arXiv preprint arXiv:2204.06125 (2022)
- [32] Ramesh, A., Pavlov, M., Goh, G., Gray, S., Voss, C., Radford, A., Chen, M., Sutskever, I.: Zero-shot text-to-image generation. In: Meila, M., Zhang, T. (eds.) Proceedings of the 38th International Conference on Machine Learning, ICML 2021, 18-24 July 2021, Virtual Event. Proceedings of Machine Learning Research, vol. 139, pp. 8821–8831. PMLR (2021), <http://proceedings.mlr.press/v139/ramesh21a.html>
- [33] Reed, S.E., Akata, Z., Yan, X., Logeswaran, L., Schiele, B., Lee, H.: Generative adversarial text to image synthesis. In: Balcan, M., Weinberger, K.Q. (eds.) Proceedings of the 33rd International Conference on Machine Learning, ICML 2016, New York City, NY, USA, June 19-24, 2016. JMLR Workshop and Conference Proceedings, vol. 48, pp. 1060–1069. JMLR.org (2016), <http://proceedings.mlr.press/v48/reed16.html>
- [34] Rombach, R., Blattmann, A., Lorenz, D., Esser, P., Ommer, B.: High-resolution image synthesis with latent diffusion models. In: IEEE/CVF Conference on Computer Vision and Pattern Recognition, CVPR 2022, New Orleans, LA, USA, June 18-24, 2022. pp. 10674–10685. IEEE (2022). <https://doi.org/10.1109/CVPR52688.2022.01042>, <https://doi.org/10.1109/CVPR52688.2022.01042>
- [35] Saharia, C., Chan, W., Saxena, S., Li, L., Whang, J., Denton, E.L., Ghasemipour, S.K.S., Lopes, R.G., Ayan, B.K., Salimans, T., Ho, J., Fleet, D.J., Norouzi, M.: Photorealistic text-to-image diffusion models with deep language understanding. In: NeurIPS (2022), http://papers.nips.cc/paper_files/paper/2022/hash/ec795aeadae0b7d230fa35cbaf04c041-Abstract-Conference.html
- [36] Sandler, M., Howard, A., Zhu, M., Zhmoginov, A., Chen, L.C.: Mobilenetv2: Inverted residuals and linear bottlenecks. In: Proceedings of the IEEE conference on computer vision and pattern recognition. pp. 4510–4520 (2018)
- [37] Scheffer, T., Decomain, C., Wrobel, S.: Active hidden Markov models for information extraction. In: Proceedings of the International Symposium on Intelligent Data Analysis (2001)
- [38] Sener, O., Savarese, S.: Active learning for convolutional neural networks: A core-set approach. In: 6th International Conference on Learning Representations, ICLR 2018, Vancouver, BC, Canada, April 30 - May 3, 2018, Conference Track Proceedings. OpenReview.net (2018), <https://openreview.net/forum?id=H1aIuk-RW>
- [39] Settles, B.: Active learning literature survey (2009)
- [40] Shannon, C.E.: A mathematical theory of communication. ACM SIGMOBILE mobile computing and communications review **5**(1), 3–55 (2001)
- [41] Simonyan, K., Zisserman, A.: Very deep convolutional networks for large-scale image recognition. arXiv preprint arXiv:1409.1556 (2014)
- [42] Sohl-Dickstein, J., Weiss, E.A., Maheswaranathan, N., Ganguli, S.: Deep unsupervised learning using nonequilibrium thermodynamics. In: Bach, F.R., Blei, D.M. (eds.) Proceedings of the 32nd International Conference on Machine Learning, ICML 2015, Lille, France, 6-11 July 2015. JMLR Workshop and Conference Proceedings, vol. 37, pp. 2256–2265. JMLR.org (2015), <http://proceedings.mlr.press/v37/sohl-dickstein15.html>

- [43] Trabucco, B., Doherty, K., Gurinas, M., Salakhutdinov, R.: Effective data augmentation with diffusion models. arXiv preprint arXiv:2302.07944 (2023)
- [44] Tran, T., Do, T., Reid, I.D., Carneiro, G.: Bayesian generative active deep learning. In: Chaudhuri, K., Salakhutdinov, R. (eds.) Proceedings of the 36th International Conference on Machine Learning, ICML 2019, 9-15 June 2019, Long Beach, California, USA. Proceedings of Machine Learning Research, vol. 97, pp. 6295–6304. PMLR (2019), <http://proceedings.mlr.press/v97/tran19a.html>
- [45] Wang, K., Zhang, D., Li, Y., Zhang, R., Lin, L.: Cost-effective active learning for deep image classification. *IEEE Trans. Circuits Syst. Video Technol.* **27**(12), 2591–2600 (2017). <https://doi.org/10.1109/TCSVT.2016.2589879>, <https://doi.org/10.1109/TCSVT.2016.2589879>
- [46] Wu, C., Liang, J., Ji, L., Yang, F., Fang, Y., Jiang, D., Duan, N.: Nüwa: Visual synthesis pre-training for neural visual world creation. In: Avidan, S., Brostow, G.J., Cissé, M., Farinella, G.M., Hassner, T. (eds.) Computer Vision - ECCV 2022 - 17th European Conference, Tel Aviv, Israel, October 23-27, 2022, Proceedings, Part XVI. Lecture Notes in Computer Science, vol. 13676, pp. 720–736. Springer (2022). https://doi.org/10.1007/978-3-031-19787-1_41, https://doi.org/10.1007/978-3-031-19787-1_41
- [47] Xu, T., Zhang, P., Huang, Q., Zhang, H., Gan, Z., Huang, X., He, X.: Attngan: Fine-grained text to image generation with attentional generative adversarial networks. In: 2018 IEEE Conference on Computer Vision and Pattern Recognition, CVPR 2018, Salt Lake City, UT, USA, June 18-22, 2018. pp. 1316–1324. Computer Vision Foundation / IEEE Computer Society (2018). <https://doi.org/10.1109/CVPR.2018.00143>, http://openaccess.thecvf.com/content_cvpr_2018/html/Xu_AttnGAN_Fine-Grained_Text_CVPR_2018_paper.html
- [48] Yang, L., Zhang, Z., Song, Y., Hong, S., Xu, R., Zhao, Y., Zhang, W., Cui, B., Yang, M.H.: Diffusion models: A comprehensive survey of methods and applications. *ACM Computing Surveys* (2022)
- [49] Yin, Y., Kaddour, J., Zhang, X., Nie, Y., Liu, Z., Kong, L., Liu, Q.: Ttida: Controllable generative data augmentation via text-to-text and text-to-image models. arXiv preprint arXiv:2304.08821 (2023)
- [50] Yoo, D., Kweon, I.S.: Learning loss for active learning. In: IEEE Conference on Computer Vision and Pattern Recognition, CVPR 2019, Long Beach, CA, USA, June 16-20, 2019. pp. 93–102. Computer Vision Foundation / IEEE (2019). <https://doi.org/10.1109/CVPR.2019.00018>, http://openaccess.thecvf.com/content_CVPR_2019/html/Yoo_Learning_Loss_for_Active_Learning_CVPR_2019_paper.html
- [51] Yoo, D., Kweon, I.S.: Learning loss for active learning. In: Proceedings of the IEEE/CVF conference on computer vision and pattern recognition. pp. 93–102 (2019)
- [52] Yu, F., Wang, D., Shelhamer, E., Darrell, T.: Deep layer aggregation. In: Proceedings of the IEEE conference on computer vision and pattern recognition. pp. 2403–2412 (2018)
- [53] Zhan, X., Wang, Q., Huang, K.h., Xiong, H., Dou, D., Chan, A.B.: A comparative survey of deep active learning. arXiv preprint arXiv:2203.13450 (2022)
- [54] Zhang, H., Xu, T., Li, H.: Stackgan: Text to photo-realistic image synthesis with stacked generative adversarial networks. In: IEEE International Conference on Computer Vision, ICCV 2017, Venice, Italy, October 22-29, 2017. pp. 5908–5916. IEEE Computer Society (2017). <https://doi.org/10.1109/ICCV.2017.629>, <https://doi.org/10.1109/ICCV.2017.629>
- [55] Zhu, J., Bento, J.: Generative adversarial active learning. *CoRR* **abs/1702.07956** (2017), <http://arxiv.org/abs/1702.07956>
- [56] Zhu, X., Zhang, P., Lin, X., Shi, Y.: Active learning from data streams. In: Proceedings of the 7th IEEE International Conference on Data Mining (ICDM 2007), October 28-31, 2007, Omaha, Nebraska, USA. pp. 757–762. IEEE Computer Society (2007). <https://doi.org/10.1109/ICDM.2007.101>, <https://doi.org/10.1109/ICDM.2007.101>

A Detailed Experimental Settings

We present the detailed experimental parameter settings in Table 8, where ϵ denotes the constrain of regularization norm for text embedding deviation, α denotes the step size for updating the text embedding, k denotes the number of sampled images in computing the gradients during updating text embeddings, n denotes the step for updating the text embedding, B_{GAL} denotes the sampling number in GAL, and B_{AL} denotes the sampling number in AL.

In Table 1, GAAL is originally limited to binary classification on MNIST and CIFAR10 with SVM, we extend it to multi-class classification.

In Section 4.2, for each dataset, the AL baseline selects 1,000 samples per cycle from the training dataset using Margin Sampling. The GAL baseline generates $|L|$ samples per cycle using Margin Sampling, e.g., 1,000 samples for the first cycle, 2,000 samples for the second cycle, ..., and 10,000 samples for the 10-th cycle. The AL+GAL baseline selects 1,000 samples and then generates $|L|$ samples per cycle using Margin Sampling. We run 10 cycles for these baselines. In total, we have 10,000 samples for the AL and GAL baselines and 20,000 samples for the AL+GAL baseline. The fully-supervised baseline takes the whole training set of each dataset as training data.

In Section 4.3, we use the generated data set from Section 4.1 based on ResNet18 as the generated data set for other networks. Specifically, for VGG16, DenseNet121, MobileNetV2, and DLA, we run 10 cycles of active learning with the pre-generated data set. In each cycle, 1,000 samples are selected from the original training set of CIFAR10, and $|L|$ pre-generated samples are also added to the training data.

In Section 4.4, we use random sampling to randomly optimize the text embedding with different constraints of ϵ . For each setting, we generate 10 images for each class in CIFAR10 and then evaluate the accuracy of the generation. The detailed results for each class are also presented in Table 9

In Section 4.5, we evaluate the effectiveness of different components of GALOT using the default hyper-parameters as in Table 8. In the text template comparison, the text template is changed across different experiments. In the ablation study of ϵ , the ϵ is set to different values to test the effectiveness of the text embedding optimization. In the ablation study of various B_{GAL} , we change the generation number w.r.t. the cumulative labeled number $|L|$, by a factor of 0.5, 1.0, and 1.5.

Other experiment settings are also summarized in Table 8. The uncertainty presented in Table 3, Figure 5, and Figure 6 is the Standard Error of the Mean (SEM) obtained over 2 runs.

B T2I Generation Examples

B.0.1 Visual Comparisons

We first visually evaluate the quality of the zero-shot text-to-image generation. The images are generated by text-to-image models solely using the label name as input. Figure 7 provides a visual comparison between the generated images from our model and the real images across ϵ settings on CIFAR10 task. We observe that the generated images can generally match their labels, while as the ϵ increases, the visual representation deviates. Therefore, how to set up the ϵ range in active learning would be a problem since larger ϵ may provide a more diverse generation but can deviate from its class or even lead to a crashed generation. In Section 4.5, we provide some quantitative evaluation on the setting of ϵ .

Table 8: Detailed Experimental Settings

Experiment	Text Template	σ_{GAL}	σ_{AL}	N	ϵ	α	k	n	B_{AL}	B_{GAL}	Total Annotation
Table 1	a realistic photo of a {label}	MarginSampling	MarginSampling	10	linear(0, 0.5)	$\epsilon/5$	6	10	1,000	$ L $	10,000
Table 1 (basic)	{label}	MarginSampling	MarginSampling	10	0	$\epsilon/5$	6	10	1,000	$ L $	10,000
Figure 3	a realistic photo of a {label}	MarginSampling	MarginSampling	10	linear(0, 0.5)	$\epsilon/5$	6	10	1,000	$ L $	10,000
Table 2	a realistic photo of a {label}	MarginSampling	MarginSampling	10	linear(0, 0.5)	$\epsilon/5$	6	10	1,000	$ L $	10,000
Figure 7	{label}	MarginSampling	MarginSampling	1	linear(0, 0.5)	$\epsilon/5$	6	10	5,000	2,500	5,000
Figure 4	-	RandomSampling	None	10	-	$\epsilon/5$	6	10	0	100	0
Table 3	-	MarginSampling	MarginSampling	5	linear(0, 0.5)	$\epsilon/5$	6	10	1,000	0.5 $ L $	5,000
Table 4	a realistic photo of a {label}	MarginSampling	MarginSampling	5	-	$\epsilon/5$	6	10	1,000	$ L $	5,000
Figure 5	{label}	-	MarginSampling	5	linear(0, 0.5)	$\epsilon/5$	6	10	1,000	0.5 $ L $	5,000
Figure 6	{label}	MarginSampling	MarginSampling	5	linear(0, 0.5)	$\epsilon/5$	6	10	1,000	-	5,000
Table 5	a realistic photo of a {label}	MarginSampling	MarginSampling	5	linear(0, 0.5)	$\epsilon/5$	6	10	1,000	$ L $	5,000
Table 6	a realistic photo of a {label}	MarginSampling	MarginSampling	5	linear(0, 0.5)	$\epsilon/5$	6	10	1,000	-	5,000
Table 7	a realistic photo of a {label}	-	-	5	linear(0, 0.5)	$\epsilon/5$	6	10	1,000	$ L $	5,000

Table 9: Detailed Human Annotation Results (number of accurate samples in 10 generated samples)

	Template	airplane	automobile	bird	cat	deer	dog	frog	horse	ship	truck	Total
$\epsilon = 0$	"a photo of a {label}"	10	10	10	10	10	10	10	10	10	10	100
	"{label}"	10	8	9	6	10	10	10	10	5	10	88
	"a realistic photo of a {label}"	10	10	10	10	10	10	10	10	10	10	100
	"a simple photo of a {label}"	10	10	10	10	10	10	10	10	10	10	100
	"a recent photograph of a {label}"	10	10	10	10	10	10	10	10	10	10	100
	"a recent photograph of a {label }, ultra detailed, ..."	10	10	10	10	10	10	10	10	10	10	100
$\epsilon = 5$	"a photo of a {label}"	10	10	10	10	10	10	10	10	10	10	100
	"{label}"	10	1	0	3	10	0	10	10	6	10	60
	"a realistic photo of a {label}"	10	10	10	10	10	7	9	10	9	10	95
	"a simple photo of a {label}"	7	10	10	10	10	10	10	9	10	10	96
	"a recent photograph of a {label}"	10	10	10	10	10	10	10	10	10	10	100
	"a recent photograph of a {label }, ultra detailed, ..."	10	10	10	10	10	10	10	10	8	10	98
$\epsilon = 10$	"a photo of a {label}"	9	9	10	1	10	10	6	10	10	10	85
	"{label}"	8	1	3	3	2	2	10	10	0	10	49
	"a realistic photo of a {label}"	8	6	10	0	10	10	9	10	9	10	82
	"a simple photo of a {label}"	9	4	2	10	4	10	10	6	9	10	74
	"a recent photograph of a {label}"	9	10	5	7	10	10	10	2	4	10	77
	"a recent photograph of a {label }, ultra detailed, ..."	3	1	10	10	10	9	9	9	9	10	80

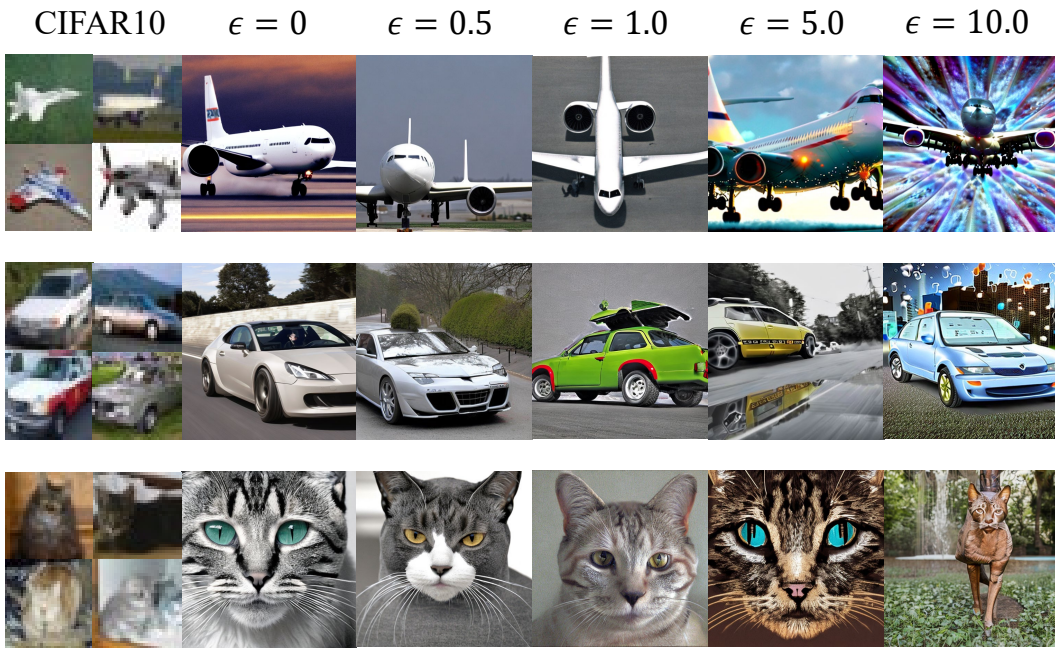


Figure 7: Visual Comparison of Generated Images VS. Real Images on CIFAR10.

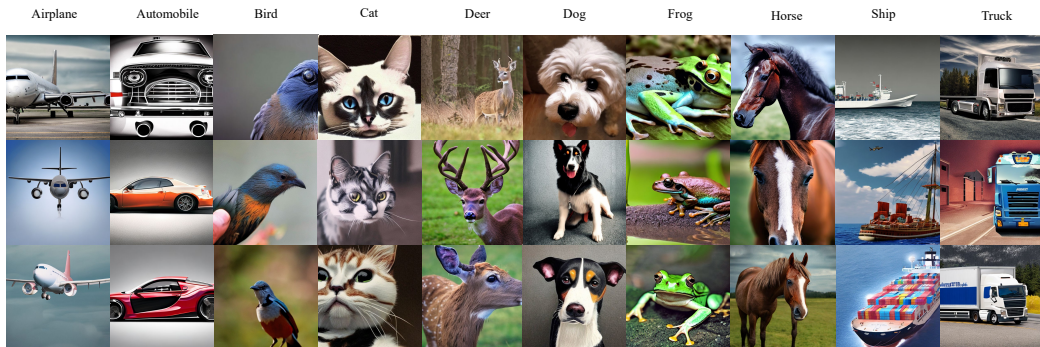


Figure 8: Generated Images for CIFAR10 Classification

To further evaluate the quality of the T2I generation, we present some examples of the generated images for different datasets in the last cycle of active learning in Section 4.1. We randomly select 3

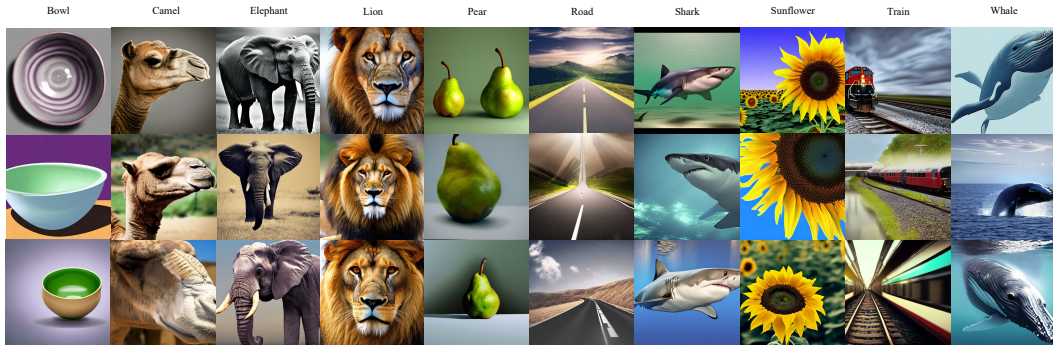


Figure 9: Generated Images for CIFAR100 Classification

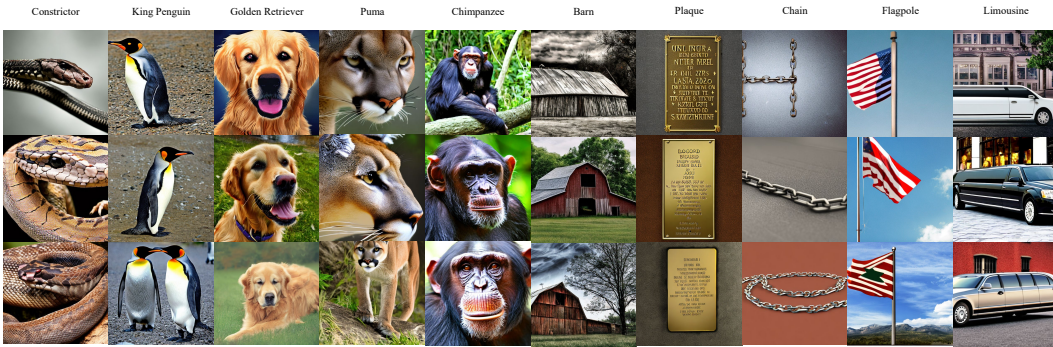


Figure 10: Generated Images for TinyImageNet Classification

images from 10 random classes of CIFAR10, CIFAR100, and TinyImageNet, presented in Figure 8, Figure 9, and Figure 10, respectively.